EDGE ARTICLE

Check for updates

Cerium-mediated site-selective cysteine functionalization

Jaewon Lee and Woon Ju Song ✶

The chemical roles of lanthanides in biology are increasingly recognized, yet remain largely unexplored. Unlike most lanthanides, cerium is redox-active and readily adapted for chemical transformation. Herein, we report a cerium-mediated oxidative thiol–ene coupling between cysteine-derived thiols and styrenes under aqueous conditions, yielding β-hydroxysulfide products. Building on this reactivity, we developed a site-selective cysteine modification strategy using a 17-amino acid cerium-binding sequence. Only cysteines optimally positioned near the vacant coordination site undergo efficient and rapid labeling, particularly with electron-deficient styrene derivatives. This work demonstrates cerium-mediated biological activity and highlights its potential as a reactive center for site-selective bioconjugation and broader biochemical and synthetic applications.

Introduction

Lanthanides, despite the misnomer as rare-earth metals, are relatively abundant in Earth's crust.[1,2] For example, the natural abundance of cerium (Ce) is comparable to that of first-row transition metals, such as cobalt, nickel, and copper,[3] making it a practical candidate for chemical applications. Lanthanides exhibit minimal variations in ionic radius and a strong preference for oxygen-donor ligands,[4] yet are distinguished by their pronounced and tunable Lewis acidity.[5,6] These properties have enabled their incorporation into organometallic complexes,[7,8] facilitating selective and versatile transformations in organic synthesis. In contrast, the biological roles of lanthanides have been relatively unexplored—aside from a few known examples such as bacterial methanol dehydrogenases[9,10]—although recent studies have revealed their accumulation in plants and microbes,[11] and identified several lanthanide-binding proteins,[12,13] including lanmodulin,[14] lanpepsy[15] and LanD.[16] These findings suggest that lanthanides may act as previously unrecognized metallocofactors in natural metalloproteins and serve as versatile elements for both biological and chemical transformations.

Among the lanthanides, Ce stands out for its unique chemical properties, exhibiting two stable oxidation states: Ce(IV) and Ce(III) under mild conditions.[17] Ce(IV) complexes have been extensively investigated for their photocatalytic reactivities,[18] often involving light-induced radical generation followed by diverse chemical transformations,[19–24] such as homolytic β-scission, C–C and C–X (X = heteroatom, such as N, O, and Cl) bond formation and decarboxylative functionalization. Ce(III),

on the other hand, displays catalytic activity as well, albeit within more limited scope. A notable example is Ce(III)-mediated oxidative C–C coupling,[25] where Ce(III)-dicarbonyl complexes generate an α-carbon radical that reacts with styrene and O_2 to produce β-hydroperoxide (Fig. 1a).[26,27] Although this Ce(III)-mediated reactivity proceeds under mild conditions, it has not yet been explored in biological systems.

Herein, we present a Ce(III)-mediated strategy for site-selective cysteine modification. Cysteine, a natural amino acid with distinctive nucleophilicity, is widely utilized as a versatile handle for bioconjugation.[28,29] However, achieving site selectivity remains challenging in most native proteins, which often contain multiple cysteine residues.[30] Recent strategies have aimed to selectively target a single cysteine within short peptide tags using specific reagents, such as the π-clamp (FCPF) with perfluoroaryl group,[31] the DBCO tag (LCYPWVY) with dibenzocyclooctyne,[32] and the CX10R7 tag (VTNQECCSIPM) with 2-cyanobenzothiazole.[33] While these methods offer high selectivity, their reliance on synthetic and bulky moieties limits broader applicability in biochemical characterization, biomimetic modeling, and therapeutic development.

In this work, we demonstrated that Ce(III) complex can mediate oxidative thiol–ene coupling under biochemically compatible conditions. By incorporating a Ce(III)-binding motif into a short peptide, we achieved high-yield, site-selective cysteine labeling. Notably, only cysteine positioned adjacent to and oriented toward the vacant site in the Ce(III) coordination sphere undergoes efficient coupling with styrene derivatives, effectively preventing non-specific modifications of other cysteine residues. The reaction yields a stable β-hydroxysulfide adduct, enabling the precise introduction of small nonbiological chemical moieties with negligible footprint. This reactivity was further extended to proteins of greater molecular

Department of Chemistry, Seoul National University, Seoul 08826, Republic of Korea. E-mail: woonjusong@snu.ac.kr
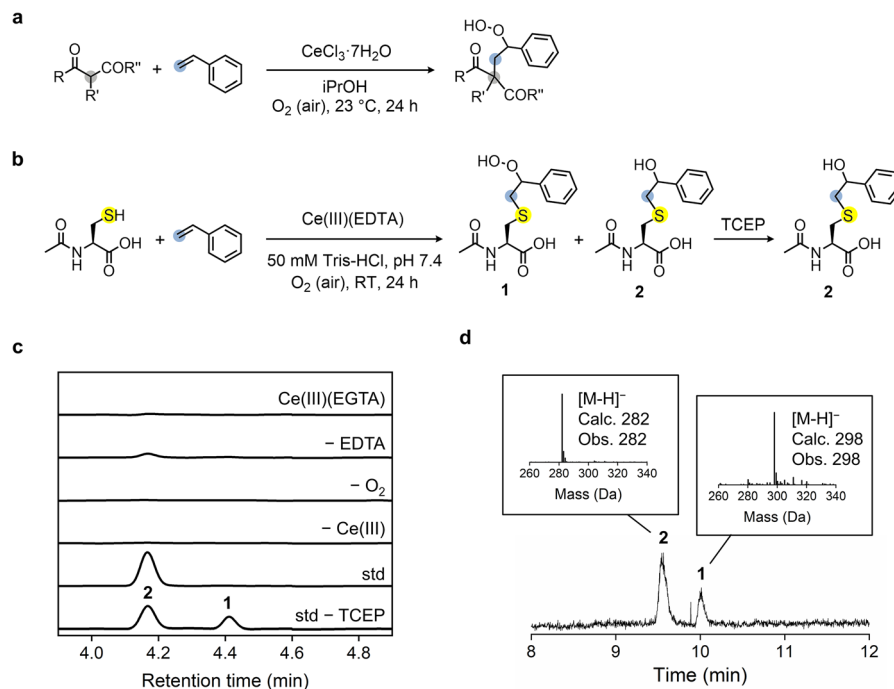
Fig. 1 Ce(III)-mediated oxidative coupling. (a) Previously reported oxidative reaction of 1,3-dicarbonyl compounds with styrene. Adapted from ref. 27. (b) Oxidative thiol–ene coupling of N-acetylcysteine (NAC) with styrene. (c) HPLC analysis. (d) LC-MS analysis of the products from the reaction shown in b before TCEP treatment.

complexity, underscoring its broad applicability in selective protein modification without compromising accuracy or efficiency.

Results and discussion

Cerium-assisted oxidative thiol–ene coupling

To evaluate whether Ce(III)-mediated oxidative thiol–ene reaction occurs under aqueous conditions, we employed N-acetylcysteine (NAC) as a cysteine surrogate, styrene as the coupling reagent, and ethylenediaminetetraacetic acid (EDTA, $\log K_{D,Ce(III)} = -16.0$)[34] as the supporting ligand (Fig. 1b). A reaction mixture containing 1 mM $CeCl_3$, 1 mM EDTA, 1 mM NAC, and 2 mM styrene, in 50 mM Tris–HCl, pH 7.4 buffer was incubated for 24 h, resulting in the formation of two products, **1** and **2** (2.8% in total), with a slow conversion from **1** to **2**. Treatment with 1 mM tris(2-carboxyethyl)phosphine (TCEP) accelerated this interconversion,[35] indicating that **2** is the reduced form of **1**. Characterizations by ^1H NMR, ^{13}C NMR, and LC-MS demonstrated that **1** is a β-hydroperoxide-adduct while **2** is a β-hydroxysulfide formed via the reduction of **1** (Fig. 1b–d, S1 and S2). Although the overall yield and reaction rate were low, the formation of **1** and **2** demonstrates a sufficient basal level of Ce(III)-mediated reactivity in this model system.

The conversion of NAC and formation of two products, **1** and **2**, was detected only in the presence of Ce(III) and molecular oxygen (Fig. 1c). Notably, no Michael addition between the thiol and styrene occurred, regardless of the reaction components present, consistent with the fact that styrene is generally considered poor Michael acceptors.[36] These data indicate that

the observed products arise from an oxidative mechanism rather than a classical nucleophilic addition. Removal of EDTA ligand significantly reduced the product yield, necessitating an ancillary ligand for Ce(III) reactivity. Replacing EDTA with an alternative multidentate ligand, ethylene glycol-bis(2-amino-ethylether)-N,N,N′,N′-tetraacetic acid (EGTA), which favors a higher coordination number of eight[37] compared to that of EDTA with six,[38] resulted in no detectable product formation. These results suggest that the presence of a coordinatively vacant site in the Ce(III) complex is critical for facilitating the oxidative thiol–ene coupling.

Design of lanthanide-binding peptides for oxidative thiol–ene coupling

Building on the basal level of activity observed with the Ce(III)(EDTA) complex, we designed a Ce(III)-binding peptide to extend oxidative thiol–ene coupling reactivity. Two well-characterized lanthanide-binding motifs were considered: the three EF-hands (EF1–3) of lanmodulin from *M. extorquens* AM1 (*Mex*-LanM)[14] and a lanthanide-binding tag (LBT)[39] reported previously (Fig. 2a and b). Both motifs are 12-amino acid sequences, predominantly composed of acidic residues—aspartate and glutamate—at the first, third, fifth, and twelfth positions of the EF-hands, corresponding to D_1, D_3, D_5, and E_{12} in *Mex*-LanM EF3, respectively (subscript for the numbering scheme in EF-hands).

Notable sequence differences between *Mex*-LanM and LBT are observed at the second, third, and ninth positions of the EF-motifs. In *Mex*-LanM, a proline at the second position induces
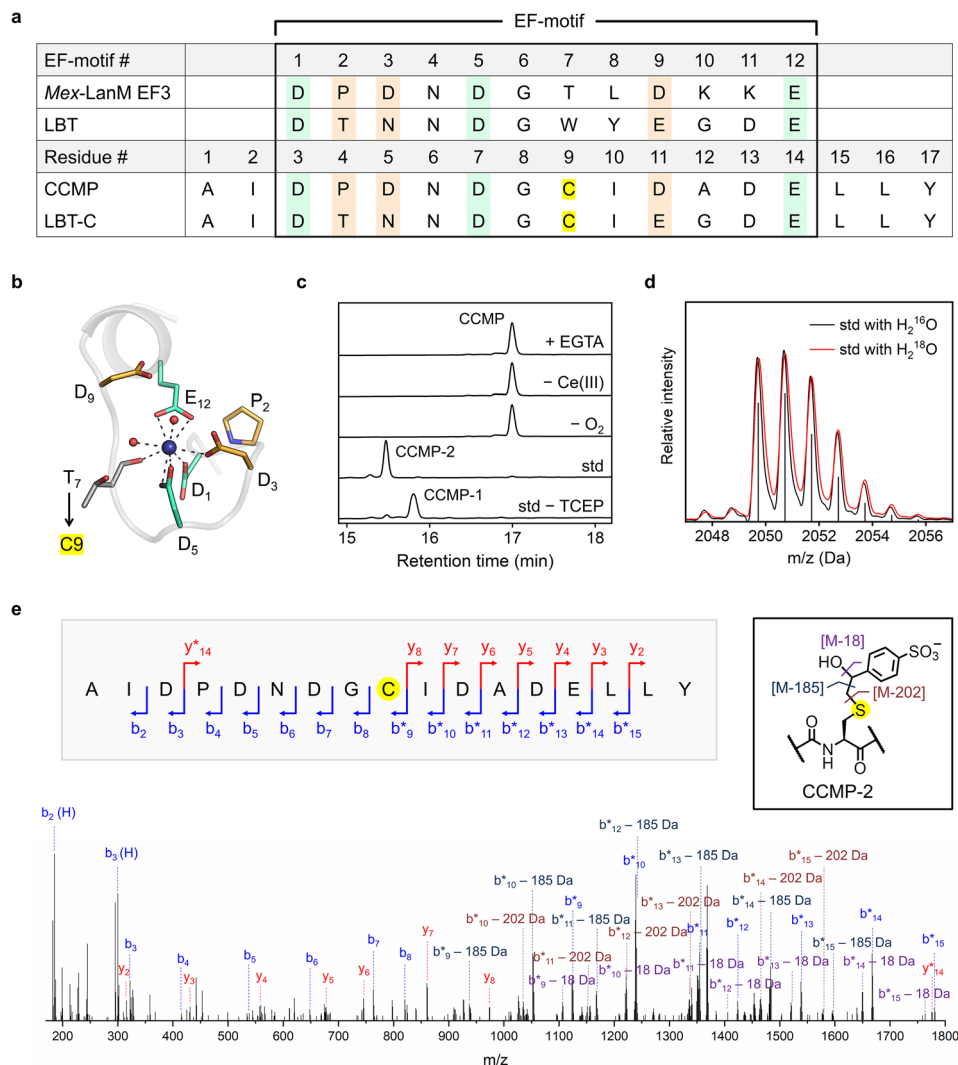
Fig. 2 Design of Ce(III)-binding peptides for site-specific oxidative thiol–ene coupling. (a) Amino acid sequences of *Mex*-LanM EF3, LBT, and CCMP mutants. EF-hand motifs are highlighted with a bold-bordered box. (b) A previously reported X-ray crystal structure of the 3rd EF-hand of *Mex*-LanM (PDB code: 8fns). Metal (Nd(III) in this case) and metal-bound water molecules are shown with blue and red spheres, respectively. (c) HPLC analysis of the reactions with 100 μM Ce(III)(CCMP) and 10 mM 4VBS in 50 mM Tris–HCl, pH 7.4, followed by 1 mM TCEP treatment and the modified conditions. (d) Negative-ion mode MALDI-TOF/TOF analysis of CCMP-2 from the reactions with $H_2^{16}O$ or $H_2^{18}O$. Vertical drop lines indicate the calculated isotope mass distribution of CCMP-2 [M–H]⁻. (e) Tandem mass spectrometry fragmentation analysis of CCMP-2. Asterisks indicate the peptide fragments containing the modified cysteine.

a tight turn between the first and third coordinating residues and is conserved across homologs with 65% sequence identity, represented by the consensus sequence $D_1P_2D_3x$DGTZD$_9xx$E (x = arbitrary, Z = hydrophobic amino acids) (Fig. S3). This feature creates a coordinatively vacant site[40,41] (Fig. S4), analogous to that observed in the Ce(III)(EDTA) complex. In contrast, the LBT sequence, originally derived from the EF-hand superfamily—formerly known as calcium-binding motifs—features the distinct sequence $D_1x_2B_3x$DGxZx_9xxE (B = Asp or Asn), lacking highly conserved residues at the second, third, and ninth positions within EF-hands.[42] More specifically, E_9 acts as a bidentate ligand, resulting in the formation of a coordinatively saturated lanthanide complex, presumably similar to that observed with Ce(III)(EGTA).

Therefore, we hypothesize that the EF-hand motifs from *Mex*-LanM are more suitable for this work, and adopted their sequential features, along with five flanking residues at the N- and C-termini, as implemented in the LBT design[39] (Fig. 2a). A tyrosine residue was added at the C-terminus to facilitate quantification. The position for cysteine incorporation (C9) was selected based on the structural analysis (Fig. 2b): crystal structures of the LBT peptide and the EF loop of *Mex*-LanM-EF3 indicate that the seventh position (T_7), which corresponds to C9 in our design, is in close proximity and properly oriented toward the open coordination site of lanthanide-bound *Mex*-LanM,[40,43,44] at an approximate distance of 4.3 Å (Fig. S4). The resulting 17-amino acid peptide was designated as the cerium-

Table 1 Oxidative thiol–ene coupling of CCMP with 4VBS

Entry	Condition	Conv. (%)	CCMP-2 (%)	CCMP-SO_2^- (%)	Dimer (%)
1	Standard[a]	100	93	7	0
2	Ar instead of air	0	0	0	0
3	No Ce(III)	0	0	0	0
4	+10 eq. EDTA	3	3	0	0
5	+10 eq. EGTA	0	0	0	0
6	La(III) instead of Ce(III)	0	0	0	0
7	No 4VBS, 10 h	6	0	2	4
8	10 μM Ce(III)[b]	100	75	16	8
9	10 μM Ce(IV)[b]	0	0	0	0
10	10 μM Ce(IV),[b,c] 456 nm	100	71	13	10

[a] 100 μM CCMP, 100 μM $CeCl_3$, 10 mM 4VBS in 50 mM Tris–HCl, pH 7.4 buffer, 1.5 h, followed by the addition of 1 mM TCEP. [b] 10 μM CCMP, 10 μM $CeCl_3$ or $[NH_4]_2[Ce(NO_3)_6]$ (CAN), 1 mM 4VBS for 12 h. [c] Irradiated with a 456 nm LED lamp for 12 h.

dependent cysteine-modifiable peptide (CCMP) and was subjected to detect its oxidative thiol–ene reactivity (Table 1).

The Ce(III)-mediated reactivity of CCMP depends on its lanthanide-binding affinity. We therefore first characterized the coordination environment of CCMP. Terbium (Tb(III)) was used as a spectroscopic surrogate for lanthanides,[45] and its luminescence at 545 nm was monitored upon the addition of $TbCl_3$, using Förster resonance energy transfer (FRET).[46] The dissociation constant (K_D) for Tb(III) was determined with a CCMP mutant in which a tryptophan residue was introduced at the ninth position (C9W; CCMP-W). The measured K_D for Tb(III) was 0.26(5) μM, approximately four orders of magnitude higher than that of EF1–3 in *Mex*-LanM ($K_D = 2.1 \times 10^{-11}$ M)[14] (Fig. S5 and Table S3). Subsequently, an intrinsic tryptophan fluorescence-based assay was employed to assess binding affinities for other lanthanides, including Ce(III), as reported previously[47] (Fig. S7 and Table S3). The K_D value of CCMP-W for Ce(III) was determined to be 0.32(14) μM (Table 2), indicating that CCMP exhibits sufficient affinity for Ce(III) to facilitate peptide modification under micromolar conditions.

To further investigate the coordination geometry of CCMP, we conducted time-resolved luminescence experiments using Eu(III) as a surrogate metal ion, as it exhibits binding affinity comparable to that of Ce(III) in other lanthanide-binding peptides (Table S3). Lifetime measurements were used to estimate the number of coordinated water molecules (q). CCMP and CCMP-W exhibited q-values of 1.44 and 1.55, respectively (Fig. S8 and Table 2), consistent with coordination geometries similar to their parent construct, *Mex*-LanM, which typically features two water-bound sites.[40] These results suggest that the mixing of Ce(III) and CCMP spontaneously forms an *in situ* complex with an unsaturated coordination sphere, thereby fulfilling the structural prerequisite for mediating oxidative thiol–ene coupling.

Oxidative thiol–ene coupling of CCMP with styrene

We selected 4-vinylbenzenesulfonate (4VBS), a styrene analog, as the coupling partner due to its sulfonate group ($pK_a = -2.8$), which confers high water solubility (>100 mM) and compatibility with HPLC analysis (Fig. 2c and Table 1). A reaction

Table 2 Dissociation constants, kinetics constants, fluorescence lifetimes of Eu(III) and corresponding q-values of CCMP variants

CCMP variants	$K_{D,Ce(III)}$[a] (μM)	k (M^{-1} s^{-1})	τ_{H_2O} (μs)	τ_{D_2O} (μs)	q
CCMP	nd	0.11(1)	469(7)	1900(100)	1.44(5)
CCMP-W	0.32(14)	nd	392(5)	1190(70)	1.55(6)
CCMP-C10	nd	0.0083(6)	444(8)	1800(200)	1.53(9)
CCMP-C16	nd	nd	515(3)	2100(100)	1.28(4)
CCMP-D11E	0.32(8)	0.079(6)	405(3)	1160(40)	1.44(4)
CCMP-D5N	5.0(22)	0.048(2)	234(2)	510(20)	2.23(7)
CCMP-P4T	0.36(11)	0.0049(5)	481(5)	2300(100)	1.48(3)
LBT-C	0.94(30)	0.0026(6)	1274(10)	2630(70)	0.11(1)

[a] Dissociation constants were determined by adding the C9W mutation. nd: not determined.

mixture containing 100 μM CCMP, 100 μM CeCl$_3$, and 10 mM 4VBS in 50 mM Tris–HCl, pH 7.4 buffer under ambient conditions resulted in complete CCMP conversion within 1.5 h. The main product, CCMP-1, eluted at 15.8 min in the HPLC profile (Fig. 2c) and exhibited a mass increase of 216 Da relative to CCMP, as determined by LC-MS analysis. Over time, CCMP-1 gradually converted to CCMP-2, a product with a retention time of 15.5 min (Fig. S9) and a mass increase of 200 Da to CCMP (Fig. S10). Treatment with 1 mM TCEP for 1 h quantitatively converted CCMP-1 to CCMP-2 (Fig. 2c, and Table 1, entry 1). Neither CCMP-1 nor CCMP-2 product formation was observed in the absence of either O$_2$ or CeCl$_3$ (Fig. 2c and Table 1, entry 2–3). Isotope labeling experiments using H$_2$^{18}O revealed no incorporation of ^{18}O isotope into CCMP-2; the isotope distribution was identical to that of the product obtained in unlabeled water (H$_2$^{16}O) (Fig. 2d and S11). These results indicate that molecular oxygen from the ambient atmosphere, rather than water, serves as the oxidant in the oxidative thiol–ene coupling.

Characterization by ^{1}H and ^{13}C-NMR, FTIR, LC-MS, and tandem mass spectrometry indicated CCMP-2 as a β-hydroxysulfide adduct at the C9 position of CCMP, obtained in 93% yield (Fig. 2e and S10–S14). A minor byproduct (7%), identified as the sulfinic acid form (CCMP-SO$_2$$^-$), was also observed, likely arising from air oxidation of cysteine. These results indicate that Ce(III)(CCMP) exhibits reactivity analogous to Ce(III)(EDTA) but with markedly higher yields and faster kinetics, likely due to an intramolecular reaction facilitated by the spatial proximity of the cysteine and Ce(III)-binding sites within the peptide.

The addition of a 10-fold excess of the chelators EDTA or EGTA significantly suppressed the reaction, indicating that Ce(III) coordination to CCMP is essential for oxidative coupling (Fig. 2c and Table 1, entry 4–5). Furthermore, when a tripeptide lacking a Ce(III)-binding site (Gly-Cys-Phe; GCF) was used in place of CCMP, no product formation was observed (Fig. S15), and only trace amounts of coupling products (3.5% yield) were detected after 72 h. These results further support the critical role of Ce(III)-peptide coordination and the spatial proximity between the metal center and cysteine residue in promoting the reaction. Substituting Ce(III) with redox-inactive La(III), which exhibits comparable binding affinity[12] and Lewis acidity (Table S3), resulted in no product formation (Table 1, entry 6), indicating that the Lewis acidity of lanthanide ions alone is insufficient to promote the coupling reaction. In the absence of 4VBS, a 6% conversion of CCMP to oxidized forms—sulfinic acid (CCMP-SO$_2$$^-$) and a CCMP dimer—was observed after 10 h (Table 1, entry 7). Notably, these oxidized products were observed only in the presence of Ce(III), implicating its direct involvement in thiol oxidation (Fig. S16).

Ce(III)-dependent coupling reactivity was retained even at CCMP concentrations reduced tenfold, albeit with slower kinetics. A reaction containing 10 μM CeCl$_3$, 10 μM CCMP, and 1 mM 4VBS yielded 75% CCMP-2 after 12 h (Table 1, entry 8). Replacing Ce(III) with Ce(IV), which exhibits a comparable affinity ($K_{D,Ce(IV)}$ = 0.32(9) μM; Table S3), suppressed the reaction (Table 1, entry 9). However, upon exposure to blue light, product formation was restored (Table 1, entry 10). UV-Vis

spectra of the reaction mixture revealed that the characteristic Ce(IV) absorption band disappeared following irradiation, likely due to its photoreduction to Ce(III) (Fig. S17). Upon switching to green light irradiation, photoreduction was incomplete, with only 26% of Ce(IV) reduced to Ce(III) within 12 h, accompanied by 38% conversion of CCMP to CCMP-2. These results indicate that the photoinduced reduction proceeds via Ce(IV) LMCT transitions occurring in the 300–450 nm range (Fig. S17). To identify the reductants involved in photoreduction, we compared the reactivity under different buffer conditions and upon the introduction of amine-based reductants. Replacing 50 mM Tris–HCl with 50 mM borate buffer, while maintaining the pH at 8, markedly decreased both the rate and extent of Ce(IV) photoreduction, and no coupling product was detected (Fig. S18). In contrast, adding 50 mM N,N-diisopropylethylamine (DIPEA) or 1 mM 4-(dimethylamino)benzonitrile (DMABN) to the borate buffer restored Ce(III)-mediated reactivity, consistent with their role as sacrificial electron donors in Ce(IV) photoreduction (Fig. S18).

We next monitored the time-dependent conversion of CCMP during the Ce(III)-mediated oxidative coupling. The reaction rates displayed a linear dependence on the initial concentrations of Ce(III)(CCMP) and 4VBS, resulting in a second-order rate constant of 0.11 M^{-1} s^{-1} (pH 7.4, 25 °C) (Fig. S19). These rates are slower than those of previously reported cysteine modification tags, π-clamp (0.73 M^{-1} s^{-1}, pH 8, 37 °C),[31] DBCO tag (0.81 M^{-1} s^{-1}, pH 8, 37 °C)[32] and CX10R7 tag (17 M^{-1} s^{-1}, pH 7.4, 37 °C),[33] but remain suitable for biochemical applications.

Ce(III)-mediated oxidative thiol–ene coupling displayed a bell-shaped pH dependence, with maximum reactivity observed between pH 7.6 and 8.0 (Fig. S20). Two apparent pK_a values, 7.4(2) and 8.3(2), were identified, indicating the involvement of at least one deprotonation and one protonation step. One pK_a likely corresponds to the protonation state of the cysteine thiol, while the pH dependence may also be influenced by protonation of Ce(III)-bound water. Notably, at higher pH conditions, CCMP dimerization is promoted, reducing the effective concentration of monomeric CCMP available for thiol–ene coupling.

Site-specificity of cysteine modification

To investigate whether Ce(III) catalyzes thiol–ene coupling in a site-selective manner, we designed two additional CCMP variants with cysteine residues positioned at alternative sites: the 10th (CCMP-C10) or 16th positions (CCMP-C16) (Fig. 3a and b). Based on simulated structures, the distances between the C$_\beta$ of the cysteine and the bound Ce(III) ion were estimated to be 5.1 Å, 5.8 Å, and 12.6 Å for CCMP, CCMP-C10, and CCMP-C16, respectively, resulting in a 4.2 Å, 5.9 Å, and 13.0 Å distance between the metal ion and the cysteine sulfur atom, respectively (Fig. S4). Assuming that cysteine repositioning does not significantly affect the Ce(III)-coordination geometry or binding affinity, we hypothesized that the primary difference between CCMP and CCMP-C10 arises from the orientation of the thiol groups relative to the Ce(III)-binding sites, whereas the cysteine in CCMP-C16 is likely spatially separated from the metal center.
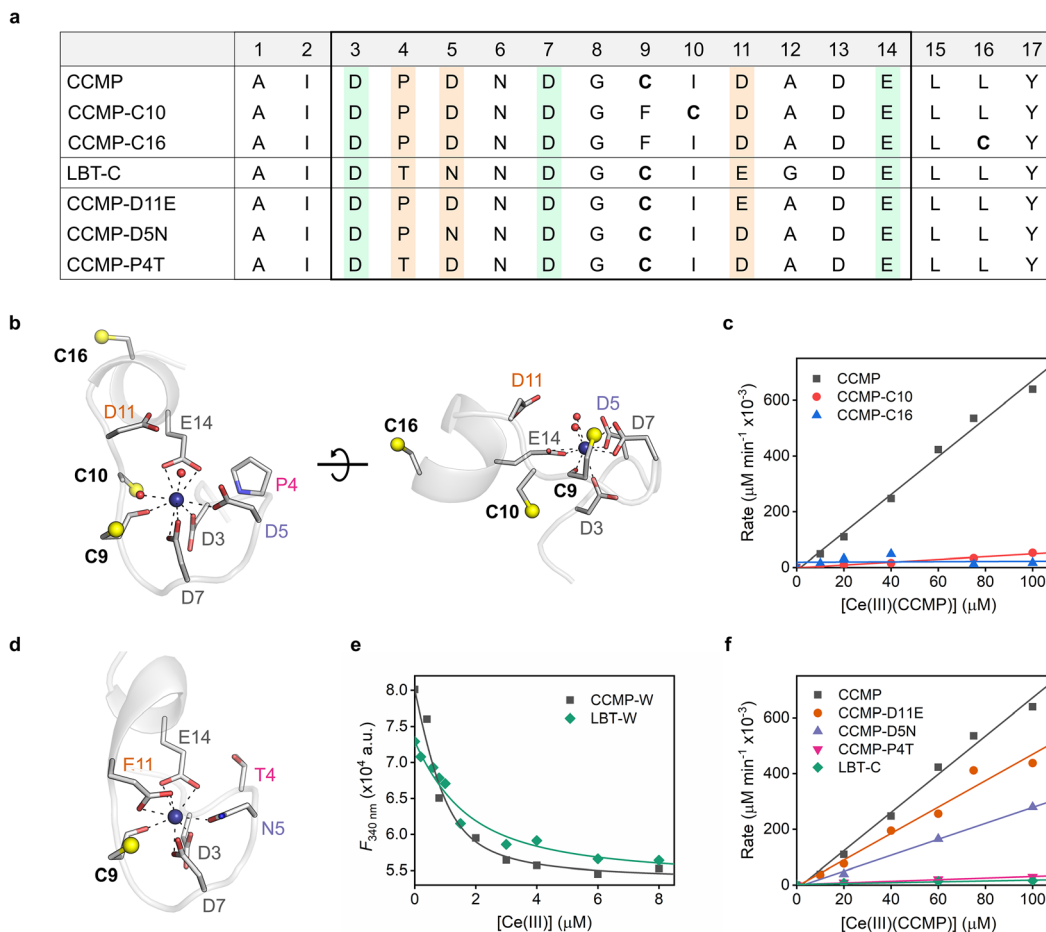
Fig. 3 Oxidative thiol–ene coupling of other Ce(III)-binding peptides. (a) Amino acid sequences of CCMP variants. EF-hand motifs are highlighted with a black box. (b) The simulated structure of CCMP using the 3rd EF-hand of *Mex*-LanM (PDB code: 8fns). (c) Kinetic analysis of CCMP cysteine mutants. (d) The simulated structure of LBT-C using LBT (PDB code: 1tjb). (e) Determination of dissociation constant ($K_{D,Ce(III)}$) by intrinsic Trp fluorescence assay using C9W mutants. (f) Kinetic analysis of CCMP mutants at the non-conserved positions. Reactions in c and f were conducted with varying concentrations of CCMP variants (10–100 μM) and a fixed concentration of 4VBS (1 mM).

The q-values, which reflect the availability of vacant coordination sites, for Ce(III)-bound CCMP-W, CCMP-C10, and CCMP-C16 are comparable to that of CCMP (Table 2), indicating that the sulfur atom of the ninth cysteine does not participate in metal coordination. Instead, the backbone carbonyl oxygen at the ninth position coordinates with the metal, a characteristic feature of EF-hand proteins,[42] likely precluding direct coordination of the cysteine sulfur to the metal center. These results also suggest that shifting the position of the cysteine residues does not substantially perturb the primary coordination sphere.

However, CCMP-C10 reacted with 4VBS at a markedly reduced rate, with a second-order rate constant of 0.008 M^{-1} s^{-1}, approximately 15-fold lower than that of CCMP (Fig. 3c and S21). Furthermore, CCMP-C16 exhibited considerably lower reactivity and no dependence on 4VBS concentration. These results indicate that Ce(III)(CCMP) exhibits high site-selectivity for cysteine residues, governed not only by the interatomic distance to the metal ion but also by the specific orientation of the thiol, likely favoring alignment toward the open coordination site of Ce(III)(CCMP).

Reactivity modulated by non-conserved sequence of CCMP

As a mechanistic probe and alternative Ce(III)-binding peptide, we introduced a cysteine at the ninth position of the LBT sequence (LBT-C) to assess its thiol–ene reactivity. LBT-C differs from CCMP at four positions: the fourth, fifth, eleventh, and twelfth residues, where proline, aspartate, aspartate, and alanine in CCMP are replaced by threonine, asparagine, glutamate, and glycine, respectively, in LBT-C (Fig. 3a and d).

The Ce(III)-binding affinity of the LBT sequence was evaluated by introducing a tryptophan residue at the ninth position (LBT-W) and performing an intrinsic tryptophan fluorescence-based assay with Ce(III), as described above (Fig. 3e and Table 2). LBT-W showed a K_D value of 0.94(30) μM for Ce(III), indicating that the four sequence differences from CCMP had minimal impact on Ce(III)-binding affinity. Time-resolved luminescence experiments using Eu(III) revealed that LBT-C exhibits a q-value of 0.11 (Fig. S8 and Table 2), consistent with a coordination geometry similar to its parent constructs, LBT[48] (Fig. S23). Finally, the oxidative coupling reactivity of LBT-C with 4VBS was significantly suppressed, with a 44-fold

decrease in the rate constant compared to CCMP (Fig. 3f and Table 2). These results suggest that variations in non-coordinating residues, even at less conserved positions, can strongly affect reactivity, likely by altering the spatial orientation or local environment around the metal center.

To further investigate the influence of the CCMP sequence, we designed additional peptide analogs with single-site substitutions at the fourth, fifth, and eleventh positions of LBT-C: CCMP-P4T, CCMP-D5N, and CCMP-D11E (Fig. 3a). Ce(III)-binding affinities of these variants were re-evaluated by introducing a tryptophan residue at the ninth position. The D11E and P4T variants exhibited K_D values comparable to that of CCMP (Table 2), whereas the D5N variant showed a reduced binding affinity, though still sufficient for experiments at sub-millimolar concentrations. The q-values of the D11E and P4T variants closely matches that of CCMP, indicating that substitution at position 11 or 4 does not alter the metal-ligation mode. In contrast, the q-value of the D5N mutant was increased to 2.23, implicating substantial structural perturbations in the primary coordination spheres.

Kinetic analysis of the CCMP variants revealed that both D11E and D5N mutations affect the reaction rate, leading to moderately reduced CCMP-2 product yields and increased dimer formation. The P4T mutation significantly impaired reactivity, reducing it to a level comparable to that of LBT-C (Fig. 3f, S22 and Table 2). The reduced reactivity of CCMP-D11E is therefore likely attributed to steric hindrance introduced by the elongated side chain of glutamate (D11E), which may obstruct access of 4VBS or dioxygen to the vacant site within the Ce(III) coordination sphere. The D5N variant incorporated an additional water molecule into the coordination sphere, and more direct perturbation at the coordination geometry may have altered the reactivity. Furthermore, the removal of proline upon P4T mutation may alter the spatial orientation of the Ce(III) center relative to the cysteine residue. Notably, the X-ray crystal structure of Gd(III)-bound LBT-tagged ubiquitin (xq-dSE3-Ub), which shares a similar sequence with CCMP-P4T and possesses either none or one water-binding site[49] (Fig. S23), supports that the presence or absence of proline at this position likely affects backbone distortion. These studies of CCMP mutants indicate that efficient oxidative thiol–ene coupling requires a precise orientation and distance between the vacant site of the Ce(III) coordination sphere and the reactive cysteine.

Mechanistic studies of Ce(III)-dependent oxidative thiol–ene coupling

Previously reported oxidative thiol–ene coupling reactions typically proceed *via* thiyl radical intermediates, initiated by UV irradiation,[50] excess peroxides,[51] transition metals,[52–54] such as Fe, Cu, Ag, and Au, and occur with specific solvents, or additives.[55] Similarly, Ce(III)-mediated oxidative C–C coupling has been proposed to involve radical intermediates.[56]

To evaluate whether the Ce(III)-mediated oxidative thiol–ene coupling is also operative *via* radical mechanism, radical trapping agents, such as 5,5-dimethyl-1-pyrroline *N*-oxide (DMPO) and α-phenyl *N*-tertiary-butyl nitrone (PBN), were added to the Ce(CCMP). No formation of any CCMP-adducts was observed (Fig. 4a and S24). Furthermore, the addition of excess radical quenchers, such as DMPO, PBN, and 2,6-di-*tert*-butyl-4-methylphenol (BHT), under standard reaction conditions, failed to suppress the oxidative coupling. Collectively, these results suggest that the Ce(III)(CCMP) complex is unlikely to form a radical species.
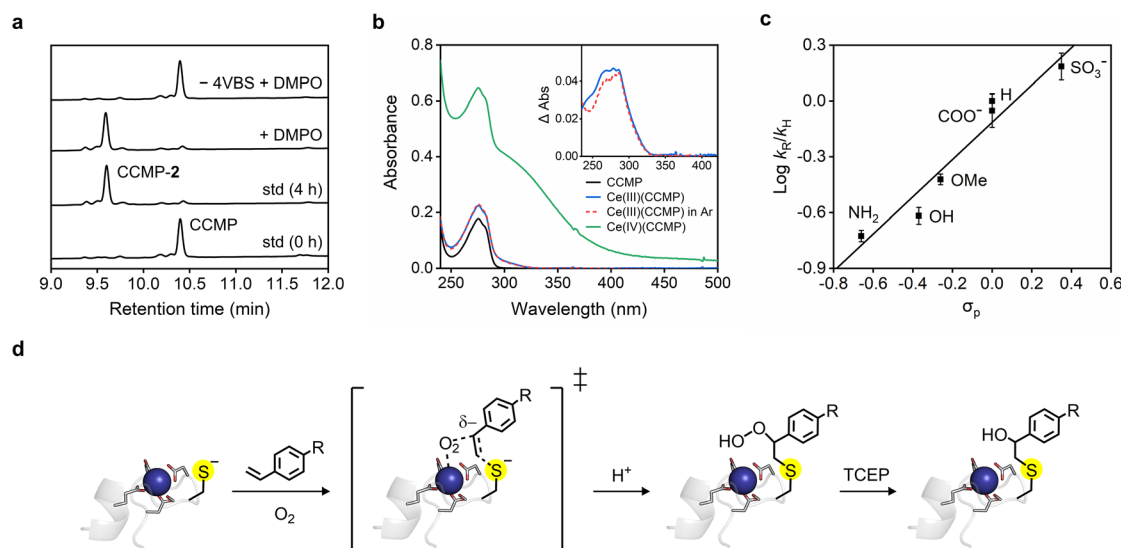

Fig. 4 Mechanistic studies of Ce(III)-mediated oxidative thiol−ene coupling. (a) HPLC analysis of the standard reaction products (0.1 mM Ce(III)(CCMP), 10 mM 4VBS in 50 mM Tris−HCl, pH 7.4) with DMPO (10 mM). (b) UV-Vis spectra of 0.1 mM CCMP complexed with 0.1 mM Ce(III) or Ce(IV) in 50 mM Tris−HCl, pH 7.4. (insert): Subtracted spectrum of 0.1 mM Ce(III)(CCMP) compared to metal-free CCMP. (c) Hammett plot analysis with *para*-substituted styrene derivatives in 50 mM Tris−HCl buffer with 10% (v/v) DMSO at pH 7.4. (d) A proposed mechanism of Ce(CCMP) with molecular oxygen and 4VBS.

We measured the UV-Vis spectra of Ce(CCMP) complexes to investigate where molecular oxygen binds to the vacant site of the Ce(III) complex. Ce(III)(CCMP) prepared under an argon atmosphere exhibited a characteristic absorption band in the 250–350 nm range (Fig. 4b, insert and Fig. S25), attributed to the 4f to 5d electronic transition of Ce(III). The UV-Vis spectrum of Ce(III)(CCMP) exposed to air was indistinguishable from that obtained under argon. Because Ce(IV)(CCMP) exhibits a distinct absorption feature in the 300–450 nm region, these data suggest that Ce(III)(CCMP) either does not readily react with dioxygen or accumulate any oxygenated intermediates under the experimental conditions.

We also measured the cyclic voltammetry (CV) of Ce(III)(CCMP) in 50 mM Tris–HCl, 150 mM NaCl, pH 7.4, revealing a quasi-reversible Ce(III)/Ce(IV) redox potential of 0.34 V vs. Ag/AgCl (3 M NaCl) (Fig. S26). This potential may not be sufficiently low to directly reduce molecular dioxygen, consistent with the absence of detectible superoxide or singlet oxygen (Fig. S27 and S28). Moreover, no correlation was observed between the Ce(III)/Ce(IV) redox potentials and the oxidative thiol–ene coupling reactivity of CCMP-P4T and LBT-C (Fig. S26). These results suggest that Ce(III) does not directly facilitate molecular oxygen reduction or induce spin state transitions associated with singlet oxygen formation.

In contrast, mixing Ce(IV)(CCMP) with an equimolar amount of potassium superoxide (KO$_2$) under anaerobic conditions led to the formation of Ce(III)(CCMP) species. Notably, CCMP, with a coordinatively unsaturated site, facilitated a substantially

faster reduction of Ce(IV) compared to LBT-C (Fig. S29). This observation suggests that reductive dioxygen activation by Ce(III) is thermodynamically unfavorable, whereas single-electron transfer from superoxide to Ce(IV) occurs more readily when a vacant coordination site is available.

We conducted a Hammett plot analysis using *para*-substituted styrene derivatives in 50 mM Tris–HCl buffer, 10% (v/v) DMSO at pH 7.4. A linear correlation with a positive slope of $\rho = 1.0(1)$ (Fig. 4c and S30) indicates that the reaction is facilitated by electron-withdrawing groups. In conjunction with the negative results from radical trapping and quenching experiments, the reaction is likely to proceed *via* a nucleophilic mechanism, in which a delocalized benzylic carbanion-like species, formed through the nucleophilic attack of a thiolate on styrene, reacts with molecular oxygen in a concerted manner (Fig. 4d). Dioxygen may participate in the reaction *via* the transient interaction with the vacant coordination site of the Ce(III) complex. While additional mechanistic or computational investigations are needed, the proposed mechanism may be analogous to that of tryptophan 2,3-dioxygenase,[57–59] wherein direct electrophilic addition of heme-bound dioxygen to the indole ring of L-tryptophan occurs without a change in the oxidation state of iron or involvement of superoxide.

Site-specific cysteine modification on CCMP-tagged ubiquitin

We expanded the reactivity of Ce(III)(CCMP)-mediated oxidative thiol–ene coupling to the protein level, targeting systems with
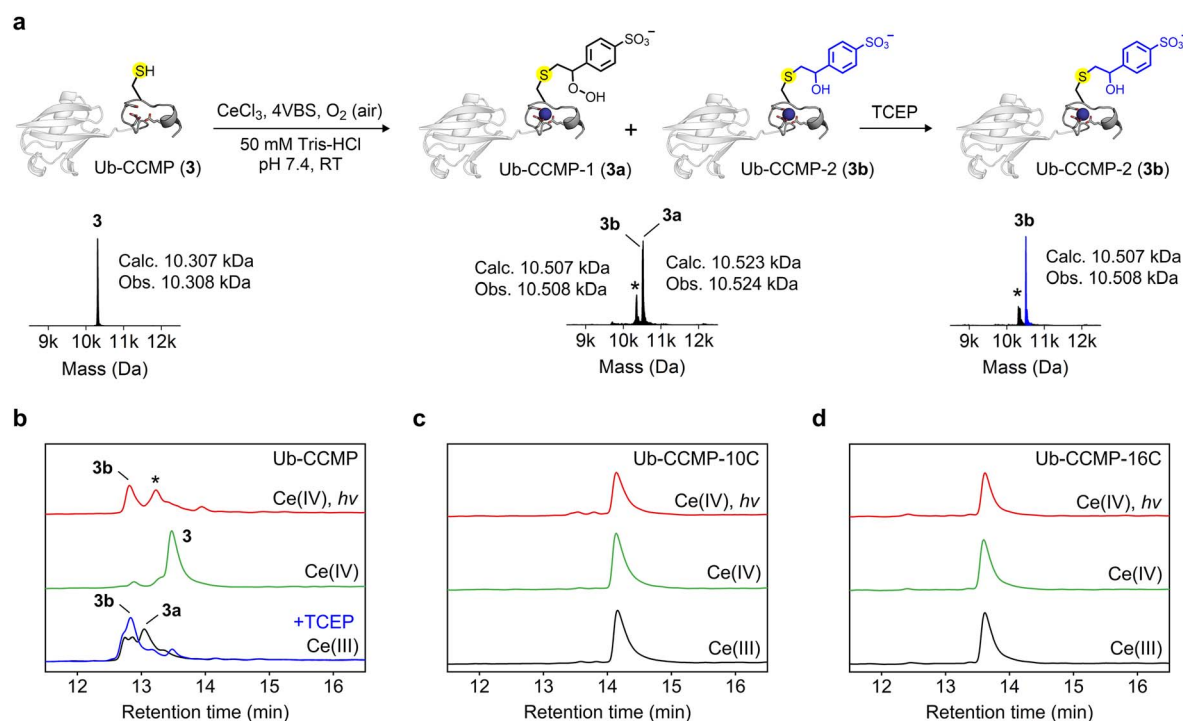

Fig. 5 Cysteine modification with 4VBS on CCMP-tagged ubiquitin. (a) A reaction scheme and LC–MS analysis. The reaction was conducted with 10 μM CeCl$_3$, 10 μM Ub-CCMP (**3**), and 1 mM 4VBS in 50 mM Tris–HCl, pH 7.4 at 25 °C for 12 h, followed by treatment with 1 mM TCEP. HPLC analysis of the reaction products after 12 h using (b) Ub-CCMP, (c) Ub-CCMP-C10, and (d) Ub-CCMP-C16. For photo-irradiated reaction, (NH$_4$)$_2$[Ce(NO$_3$)$_6$] (CAN) was used instead of CeCl$_3$ with 456 nm light. Asterisks shown in a and b indicate Ub-CCMP-SO$_2^-$ (calc. m/z = 10 339) or Ub-CCMP-SO$_3^-$ (calc. m/z = 10 355).

higher molecular complexity. We designed a chimeric protein (Ub-CCMP), consisting of ubiquitin (Ub)—a cysteine-free, 8.6 kDa regulatory protein found in most eukaryotic organisms—fused to the 17-amino acid CCMP. We created a spectroscopic analog protein (Ub-CCMP-W) by introducing a tryptophan at the 9th position of CCMP, as described above. The dissociation constant ($K_{D,Ce(III)}$ = 0.32(7) μM) was similar to those of CCMP-W (Fig. S7 and Table S3), indicating that the coordination geometry of Ce(III) remains largely unaltered upon the genetic fusion with ubiquitin.

The oxidative coupling was carried out under standard conditions with 10 μM CeCl$_3$, 10 μM Ub-CCMP (**3**) and 1 mM 4VBS. HPLC analysis demonstrated that Ub-CCMP (**3**) was completely consumed within 12 h, resulting in the formation of two primary products: Ub-CCMP-1 (**3a**) and Ub-CCMP-2 (**3b**), identified as a β-hydroperoxide and a β-hydroxy adduct, respectively. Additionally, sulfinate (Ub-CCMP-SO$_2^-$) and sulfonate (Ub-CCMP-SO$_3^-$), were observed as minor products (Fig. 5a and S31). Following treatment with TCEP, Ub-CCMP-2 (**3b**) was isolated as the major product, along with a small amount of unmodified protein, presumably regenerated through the reduction of sulfinate groups.

We also examined the photoinduced reactivity of Ce(IV)(Ub-CCMP) at the protein level. Blue light irradiation (456 nm) led to complete conversion, whereas no conversion of Ub-CCMP

was observed in the absence of irradiation (Fig. 5b and S32), consistent with the results observed for peptides (Table 1, entry 9–10). Site-specificity was further explored by shifting the cysteine residue to the 10th (Ub-CCMP-C10) or 16th positions (Ub-CCMP-C16). Neither mutant underwent protein modification with Ce(III) or Ce(IV) under blue-light irradiation (Fig. 5c, d, S33 and S34). These data highlight that Ce(III)-mediated site-specific cysteine modification is applicable to macromolecular systems with increased complexity while retaining its specificity and reactivity.

Next, we investigated the site-selectivity of Ce(III)-mediated oxidative thiol–ene coupling in proteins containing multiple cysteine residues. We introduced an additional cysteine at position K63 of ubiquitin in Ub-CCMP. To facilitate analysis, a TEV protease (TEVp) cleavage site (ENLYFQG) was also inserted between the Ub$_{K63C}$ and CCMP sequences, resulting in the construct Ub$_{K63C}$-ENLYFQG-CCMP (**4**) (Fig. 6). The coupling reaction was performed with 10 μM CeCl$_3$, 10 μM Ub$_{K63C}$-ENLYFQG-CCMP (**4**), and 10 mM 4VBS in 50 mM Tris–HCl, pH 7.4 at 25 °C for 2 h, followed by treatment with 1 mM TCEP. Nearly complete conversion of the protein to **4b** was observed, as determined by HPLC and a 200 Da mass increase in LC-MS analysis. Subsequent TEV treatment for 5 h, followed by HPLC and LC-MS analysis, revealed a 200 Da mass increase in the cleaved peptide G-CCMP-2 (**4f**), while no modification was
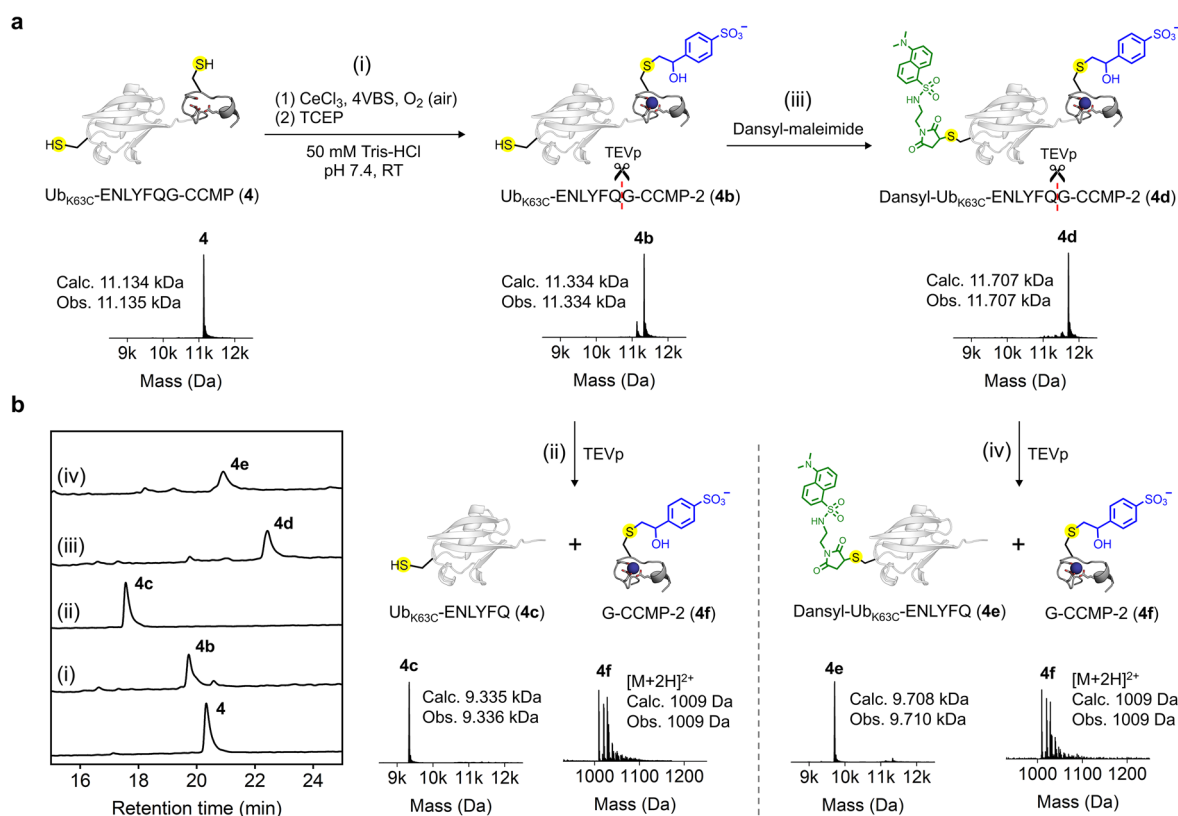

Fig. 6 One-pot dual labeling of CCMP-tagged ubiquitin with multiple cysteines. (a) A reaction scheme and LC-MS analysis. The reaction was performed by mixing with 10 μM CeCl$_3$, 10 μM **4**, and 10 mM 4VBS in 50 mM Tris–HCl, pH 7.4 at 25 °C for 2 h, followed by treatment with 1 mM TCEP. The resulting protein (**4b**) was further modified using 1 mM N-[2-(dansylamino)ethyl]maleimide. All reaction products were digested with TEV protease for analysis. (b) HPLC analysis of the modified proteins in each step.

detected in Ub$_{K63C}$-ENLYFQ (**4c**). These results indicate that the modification occurred specifically on the CCMP tag.

The modified protein **4b** was subsequently treated with 1 mM *N*-[2-(dansylamino)ethyl]maleimide (dansyl-maleimide) without purification steps. HPLC and LC-MS analysis before and after TEV protease treatment demonstrated that the dansyl adduct was introduced exclusively at the K63C position of ubiquitin (**4e**) (Fig. 6 and S35). These results demonstrate that Ce(III)-mediated thiol–ene coupling can differentiate between distinct cysteine residues within a macromolecule with high regioselectivity and precision.

Conclusions

We present the chemical reactivity of a Ce(III)-binding 17-amino acid peptide that enables site-selective cysteine modification, forming a stable β-hydroxysulfide adduct with minimal linkers and reagents. The Ce(III)-mediated oxidative thiol–ene coupling is highly dependent on both primary and secondary coordination spheres, particularly the spatial orientation and proximity of the thiol group to the metal center. Incorporation of styrene derivatives as labeling moieties expands the scope of protein modification, with potential applications in protein engineering, biosensor development, and therapeutic design. Notably, this study provides a rare demonstration of Ce(III)-mediated activity in biological systems, establishing cerium as a promising candidate for bioinspired catalysis. Furthermore, Ce(IV) enables light-controlled protein modifications, offering a versatile platform for photocrosslinking, spatiotemporal control, and optogenetic regulation.

Author contributions

J. L.: conceptualization, formal analysis, investigation, methodology, visualization, writing – original draft and review & editing. W. J. Song: conceptualization, formal analysis, investigation, funding acquisition, project administration, supervision, validation, writing – original draft, writing – review & editing.

Conflicts of interest

The authors declare no competing interests.

Data availability

The data supporting this article have been included as part of the SI. Supplementary information: Experimental procedures, SI figures and tables. See DOI: **https://doi.org/10.1039/d5sc04538j**.

Acknowledgements

Notes and references

1 J. R. Rumble, *CRC Handbook of Chemistry and Physics*, CRC Press/Taylor & Francis, Boca Raton, FL, 100th edn, 2019.

2 R. L. Rudnick and S. Gao, in *Treatise on Geochemistry*, ed. H. D. Holland and K. K. Turekian, Pergamon, Oxford, 2003, pp. 1–64.

3 A. F. Holleman and N. Wiberg, *Lehrbuch der Anorganischen Chemie*, Walter de Gruyter, Berlin, 102th edn, 2007.

4 S. Cotton, *Lanthanide and actinide chemistry*, John Wiley & Sons, 1991.

5 S. Kobayashi and K. Manabe, *Acc. Chem. Res.*, 2002, **35**, 209–217.

6 H. Pellissier, *Coord. Chem. Rev.*, 2017, **336**, 96–151.

7 M. Zimmermann and R. Anwander, *Chem. Rev.*, 2010, **110**, 6194–6259.

8 M. Nishiura, F. Guo and Z. Hou, *Acc. Chem. Res.*, 2015, **48**, 2209–2220.

9 H. Yoshihisa, A. Kentaro, A. Hiroshi, H. Makiko, I. Tomonori and K. Keiichi, *J. Biosci. Bioeng.*, 2011, **111**, 547–549.

10 F. Nanung Agus, F. Mako, M. Mika, P. Ambar, I. Tomonori and K. Keiichi, *J. Biosci. Bioeng.*, 2011, **111**, 613–617.

11 G. Tyler, *Plant Soil*, 2004, **267**, 191–206.

12 J. A. Cotruvo Jr, *ACS Cent. Sci.*, 2019, **5**, 1496–1506.

13 C. Thibault and J. S. Eric, *Science*, 2019, **363**, 489–493.

14 A. C. Joseph, R. F. Emily, A. M. Joseph, V. H. Jackson and N. L. Tatiana, *J. Am. Chem. Soc.*, 2018, **140**, 15056–15061.

15 L. H. Jethro, K. Philipp, H. Lucas, V. Thomas, M. O. Andrea, B.-M. Miriam, G. Detlef and A. V. Julia, *J. Biol. Chem.*, 2023, **299**, 102940.

16 W. B. Larrinaga, J. J. Jung, C.-Y. Lin, A. K. Boal and J. A. Cotruvo, *Proc. Natl. Acad. Sci. U. S. A.*, 2024, **121**, e2410926121.

17 A. P. Nicholas, R. R. Jerome, J. W. Patrick and J. S. Eric, *Coord. Chem. Rev.*, 2014, **260**, 21–36.

18 Y. Qiao and E. J. Schelter, *Acc. Chem. Res.*, 2018, **51**, 2926–2936.

19 J.-J. Guo, A. Hu, Y. Chen, J. Sun, H. Tang and Z. Zuo, *Angew. Chem., Int. Ed.*, 2016, **55**, 15319–15322.

20 H. Anhua, G. Jing-Jing, P. Hui and Z. Zhiwei, *Science*, 2018, **361**, 668–672.

21 Y. Qiaomu, W. Yu-Heng, Q. Yusen, G. Michael, J. C. Patrick, J. W. Patrick and J. S. Eric, *Science*, 2021, **372**, 847–852.

22 Y. Abderrazak, A. Bhattacharyya and O. Reiser, *Angew. Chem., Int. Ed.*, 2021, **60**, 21100–21115.

23 A. S. Klein, F. Leiss-Maier, R. Mühlhofer, B. Boesen, G. Mustafa, H. Kugler and C. Zeymer, *J. Am. Chem. Soc.*, 2024, **146**, 25976–25985.

24 J. Du, X. Yang, X. Wang, Q. An, X. He, H. Pan and Z. Zuo, *Angew. Chem., Int. Ed.*, 2021, **60**, 5370–5376.

25 J. Christoffers, T. Werner and M. Rössle, *Catal. Today*, 2007, **121**, 22–26.

26 J. Christoffers, T. Werner, W. Frey and A. Baro, *Eur. J. Org Chem.*, 2003, **2003**, 4879–4886.

27 M. Rössle, T. Werner, A. Baro, W. Frey and J. Christoffers, *Angew. Chem., Int. Ed.*, 2004, **43**, 6547–6549.

28 S. B. Gunnoo and A. Madder, *ChemBioChem*, 2016, **17**, 529–553.

29 J. M. Chalker, G. J. L. Bernardes and B. G. Davis, *Acc. Chem. Res.*, 2011, **44**, 730–741.

30 T. U. Consortium, *Nucleic Acids Res.*, 2022, **51**, D523–D531.

31 C. Zhang, M. Welborn, T. Zhu, N. J. Yang, M. S. Santos, T. Van Voorhis and B. L. Pentelute, *Nat. Chem.*, 2016, **8**, 120–128.

32 C. Zhang, P. Dai, A. A. Vinogradov, Z. P. Gates and B. L. Pentelute, *Angew. Chem., Int. Ed.*, 2018, **57**, 6459–6463.

33 C. P. Ramil, P. An, Z. Yu and Q. Lin, *J. Am. Chem. Soc.*, 2016, **138**, 5499–5502.

34 R. M. Smith and A. E. Martell, *Sci. Total Environ.*, 1987, **64**, 125–147.

35 D. B. Denney, W. F. Goodyear and B. Goldstein, *J. Am. Chem. Soc.*, 1960, **82**, 1393–1395.

36 D. P. Nair, M. Podgórski, S. Chatani, T. Gong, W. Xi, C. R. Fenoli and C. N. Bowman, *Chem. Mater.*, 2014, **26**, 724–744.

37 S. Aime, A. Barge, A. Borel, M. Botta, S. Chemerisov, A. E. Merbach, U. Müller and D. Pubanz, *Inorg. Chem.*, 1997, **36**, 5104–5112.

38 A. Smerigan, S. Biswas, F. D. Vila, J. Hong, J. Perez-Aguilar, A. S. Hoffman, L. Greenlee, R. B. Getman and S. R. Bare, *Inorg. Chem.*, 2023, **62**, 14523–14532.

39 N. Mark, S. Manashi, J. F. Katherine, P. Ezra, N. A. Karen and I. Barbara, *Angew. Chem., Int. Ed.*, 2004, **43**, 3682–3685.

40 J. A. Mattocks, J. A. Cotruvo and G. J. P. Deblonde, *Chem. Sci.*, 2022, **13**, 6054–6066.

41 E. C. Cook, E. R. Featherston, S. A. Showalter and J. A. Cotruvo Jr, *Biochemistry*, 2019, **58**, 120–125.

42 J. L. Gifford, M. P. Walsh and H. J. Vogel, *Biochem. J.*, 2007, **405**, 199–221.

43 A. M. Joseph, J. J. Jonathan, L. Chi Yun, D. Ziye, H. Y. Neela, R. F. Emily, S. K.-Y. Christina, A. H. Timothy, M. P. Dan, K. B. Amie and A. C. Joseph, *Nature*, 2023, **618**, 87–93.

44 E. R. Featherston, E. J. Issertell and J. A. Cotruvo Jr, *J. Am. Chem. Soc.*, 2021, **143**, 14287–14299.

45 J.-C. G. Bünzli, *Chem. Rev.*, 2010, **110**, 2729–2755.

46 A. M. Joseph, L. T. Jonathan and A. C. Joseph, in *Rare-Earth Element Biochemistry: Characterization and Applications of Lanthanide-Binding Biomolecules*, ed. A. C. Joseph, Academic Press, 2021, vol. 651, pp. 23–61.

47 R. W. Ricci and K. B. Kilichowski, *J. Phys. Chem.*, 1974, **78**, 1953–1956.

48 K. Barthelmes, A. M. Reynolds, E. Peisach, H. R. A. Jonker, N. J. DeNunzio, K. N. Allen, B. Imperiali and H. Schwalbe, *J. Am. Chem. Soc.*, 2011, **133**, 808–819.

49 K. D. Daughtry, L. J. Martin, A. Sarraju, B. Imperiali and K. N. Allen, *ChemBioChem*, 2012, **13**, 2567–2574.

50 A. L. J. Beckwith and R. D. Wagner, *J. Org. Chem.*, 1981, **46**, 3638–3645.

51 M. S. Kharasch, W. Nudenberg and G. J. Mantell, *J. Org. Chem.*, 1951, **16**, 524–532.

52 H. Xi, B. Deng, Z. Zong, S. Lu and Z. Li, *Org. Lett.*, 2015, **17**, 1180–1183.

53 A. K. Singh, R. Chawla, T. Keshari, V. K. Yadav and L. D. S. Yadav, *Org. Biomol. Chem.*, 2014, **12**, 8550–8554.

54 A. On-Yee Chan, J. Lui-Lui Tsai, V. Kar-Yan Lo, G.-L. Li, M.-K. Wong and C.-M. Che, *Chem. Commun.*, 2013, **49**, 1428–1430.

55 K. Choudhuri, A. Mandal and P. Mal, *Chem. Commun.*, 2018, **54**, 3759–3762.

56 J.-M. Speldrich and J. Christoffers, *Eur. J. Org Chem.*, 2021, **2021**, 907–914.

57 M. Sono, M. P. Roach, E. D. Coulter and J. H. Dawson, *Chem. Rev.*, 1996, **96**, 2841–2888.

58 S. J. Thackray, C. G. Mowat and S. K. Chapman, *Biochem. Soc. Trans.*, 2008, **36**, 1120–1123.

59 R. Makino, E. Obayashi, H. Hori, T. Iizuka, K. Mashima, Y. Shiro and Y. Ishimura, *Biochemistry*, 2015, **54**, 3604–3616.